JOURNAL OF MATERIALS SCIENCE 2 (1967) 378–387

Etching Studies of Beryllium Oxide Crystals

S. B. AUSTERMAN
Atomics International, Canoga Park, California, USA
J. B. NEWKIRK
University of Denver, Denver, Colorado, USA
D. K. SMITH, H. W. NEWKIRK
Lawrence Radiation Laboratory, Livermore, California, USA

Received 17 April 1967

Chemical etching behaviour of BeO crystals was investigated for selected etchants ranging from basic to acidic in nature. Surface-emergent defects (dislocations, enclosed platinum crystals, point-defect concentrations, surface mechanical damage, twin boundaries) give rise to recognisable etch figures that are characteristic of etchant, defect type, and orientation of emergence face. Gross etching rates (in the absence of surface-emergent defects) are strongly anisotropic for both basic and acidic etchants, reflecting the crystallographic polarity of the BeO crystal structure; intermediate etchants give nearly isotropic etching. The details of gross and figure etching are described.

1. Introduction

The usefulness of etching techniques to the study of surface-emergent crystal defects is well recognised [1]. These techniques have had widespread application in material studies [2], although they have not been seriously applied to BeO. Chemical etchants have been used for treating polished sections of polycrystalline BeO for microscopic examination (for example [3]). Several papers have briefly described the results of limited etching experience with single crystals [4-6]. Only in a recent report [7], devoted to etching of dislocations with hydrofluosilicic acid, has there been any attempt to make specific correlation between crystal morphology or orientation, surface-emergent crystal defects, and character of the etchant.

The objective of the present studies was to evaluate a limited number of potentially useful etchants for application to revealing surface-emergent crystal defects in BeO. This objective was sought with single crystals, using X-ray diffraction topography and optical microscopy as auxiliary methods of defect identification. It should be noted that these results may not be entirely applicable to etching of polycrystalline BeO ceramic, because of the more complex defect array expected in the latter. Familiarity with the relatively unambiguous results with crystals, though, is expected to contribute significantly to interpretation of etch figures on polycrystalline material. These data on etchants and resulting etch figures also will contribute to further studies on physical properties of BeO in crystal form.

2. Experimental Procedures

BeO crystals grown from solution in lithium polymolybdate were used in these studies, both in as-grown form and as cut and polished along various crystal planes. Although a wide variety of crystal growth forms have been observed, the most common crystal habits are prismatic, pyramidal, and plate-like. The common crystal faces are (00.1), {10.1}, {10.0}; and a sloping curved face vicinal to (00.$\bar{1}$) [8, 9].

Several crystals were ground to spherical shape. First they were ground to approximately spherical shape, and then shaped to the final geometry using a dual motor grinder with three-point suspension of the ball.*

The crystal structure of BeO is of the wurtzite type and thus is polarised along the *c*-axis [4]. All crystals examined contained inversion

*Scott Lapidary Equipment Co, Beaumont, California, USA

twins [10], with boundaries emergent on the growth face, separating basal plane areas of opposing polarity; occasionally, the twin boundary also was emergent on prism faces as noted below. Other characteristic defect structures previously noted by visual examination or X-ray diffraction topography include an axial screw dislocation, stratified point-defect concentrations, and enclosed Pt crystals [11]. Many of these features, as well as crystal morphology, are illustrated in fig. 1.

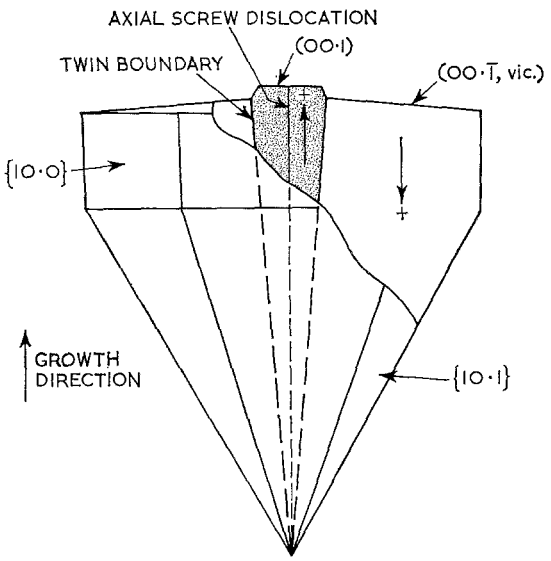

Figure 1 Cut-away diagram of typical symmetrical crystal showing geometry of crystal polarities, inversion twin, external morphology, and axial screw dislocation.

The etchants (except the hydroxides) were heated in Pt crucibles. The crystals were submerged in the noted etchants at controlled temperatures and times, with the crystals suspended in Pt, wire or foil, baskets. Molten NaOH and KOH were heated in Ni crucibles; aqueous NaOH was contained in ordinary laboratory glassware. The etched surfaces were examined by optical microscopy and Nomarski contrast interferometry [12]. These observations and X-ray diffraction topography were used to establish correspondence between crystal defect structures, etch figures, and dissolution phenomena.

For conciseness in presentation, the bulk of these observations is summarised in appendix 1. Appendix 2 lists those chemicals found to be unreactive toward BeO crystal surfaces under the conditions noted. Only the more significant aspects of the etching and dissolution phenomena are described in the following sections.

3. General Chemical Etching

We consider here the chemical interactions between the etchant and the various common crystal faces, in the presumed absence of crystal defects. Modification, by the defects, of this general chemical interaction will be considered in the following sections.

The etchants used ranged from acidic to basic in chemical nature. The principal representative of the acidic etchants is phosphoric acid (H_3PO_4), although HF also was investigated briefly. For convenience, we will designate acidic etchants as "class I".

The acidic etchants are highly selective between the positive (Be) and negative (O) basal planes, in that the former shows no etching effect and the latter is rapidly attacked. The most rapidly attacked faces are the pyramidal faces, especially {10.1}, and the most resistant (along with (00.1)) is the prismatic face, {10.0}. On (00.1) and {10.0}, any etching taking place is attributable to surface-emergent defects as described below; on all other faces, etching morphology is only modified by the defects.

Basic etchants behave oppositely to acidic etchants, in that basic etchants attack the *positive* face most rapidly. It will be noted in a later section that the attack on (00.1) is further accentuated in the vicinity of an emergent screw dislocation or an inversion twin boundary. On all other common crystal faces, there is general, non-selective, etching attack with a significant rate of dissolution and with rounding of corners.

The principal representative of the basic etchants is a series of molten salts based upon Li_2MoO_4 as the principal component. To this is added MoO_3, $Na_2B_4O_7$, $LiBO_2$, or V_2O_5 in various amounts from 2 to 100% by weight. Crystals submerged in only the principal component, Li_2MoO_4, for $\frac{1}{2}$ h at 800° C show no visible sign of etching; the solvent action in the mixed etchants, therefore, can only be attributed to the presence of the additives. This etchant series is designated for convenience as "class II". NaOH and KOH are also basic, but differ somewhat in detail in etching behaviour in BeO.

A third important type of etchant can be

used as a non-selective but active etchant. It also is based on Li_2MoO_4 as a principal component, although in this case the additive is a phosphate compound. $NaPO_3$ was used as the additive for the results reported here; P_2O_5 as additive yielded the same general behaviour. The composition $Li_2MoO_4/NaPO_3$ in equal weight proportions will be termed "class-III" etchant. All exposed crystal surfaces are attacked, although possibly not equally, and corners are rounded by this etchant. Emergent crystal defects are not revealed by this class of etchants; in fact, etch figures previously developed at defects by class-I or class-II etchants can be erased readily by etching in the composition just noted. The average surface removal rate is approximately 40 μm/h at 800° C; this is rapid enough to remove, within $\frac{1}{2}$ h or less of etching time, virtually all surface damage, due to casual intercrystal abrasion or cut-and-polish operations, that can be detected by X-ray diffraction topography. At 1100° C, etchants in this class become polishing agents.

The gross etching interrelation between crystallographic orientation of exposed surface, polar orientation, and character of etchant is well illustrated by etching the spherically ground crystals in H_3PO_4. A sphere presents a convex surface of all orientations to the etchant, and the resultant dissolution shape is bounded by the fastest-etching shapes. Fig. 2 shows typical sphere morphology after prolonged etching in H_3PO_4 at 170° C. The fastest-etching planes are $(00.\bar{1})$, {10.1}, and {11.1}, with {11.1} being somewhat slower than the other two, as evidenced on the etched spheres. Dissolution is nil on (00.1), {10.0}, and {11.0}, and on negative pyramidal planes which are approximately 45° from $(00.\bar{1})$. Spheres etched to their limiting form approach the form of positive hexagonal hemipyramids containing no Be-rich faces. This result is in agreement with predictions based on the surface bonding model discussed earlier [4].

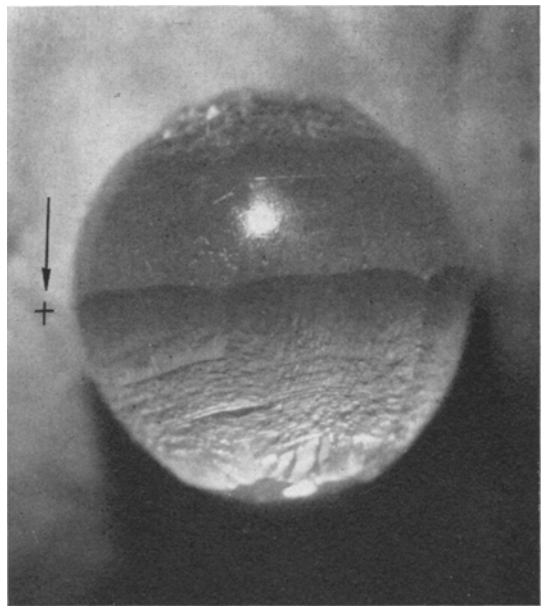

Figure 2 BeO crystal sphere after prolonged etching in H_3PO_4 (×10).

4. Etching at Defects

4.1. Dislocations

The only type of dislocation consistently observed by X-ray diffraction topography is an axial screw dislocation [10], primarily in the prismatic and pyramidal crystals. Emergence of the axial screw dislocation on the positive basal plane face is revealed by pits formed by class-II etchants. A 10 min etch in $Li_2MoO_4/2\%$ $LiBO_2$, at 800° C, for example, produced a sharp-bottomed pit (fig. 3), about 10 μm across, at the dislocation. Occasionally, families of curved dislocations arising from inclusions in the crystal bulk are found. At the points of emergence on $(00.\bar{1}$ vic.*), class-II etchants produce pits on these dislocations. Although edge dislocations emergent on non-basal faces occasionally were observed in platelet crystals,

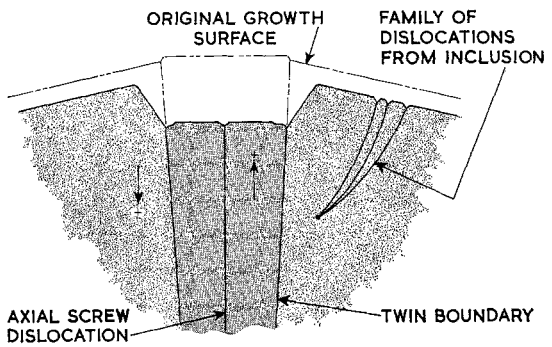

Figure 3 Sketch of etching morphology of growth face after prolonged etching in $Na_2B_4O_7/Li_2MoO_4$ with formation of crater, grooves and terrace at the twin boundary, and pits at emergent dislocations.

*vicinal

no investigation of associated etch-figures was made.

Fresh edge dislocations emergent on {10.0} yield etch pits in class-II etchants. Evidence for this conclusion was the etching development of a band of pits along any deliberately introduced, mechanical scratch, as shown in fig. 4. The presumption that edge dislocations were formed and moved along basal slip planes is consistent with the etch-pit pattern observed here, as well as with prior deformation studies by Bentle and Miller [13]. The work by Vandervoort and Barmore deals more extensively with etch pits centred on dislocations, primarily those freshly introduced, with hydrofluosilicic acid [7].

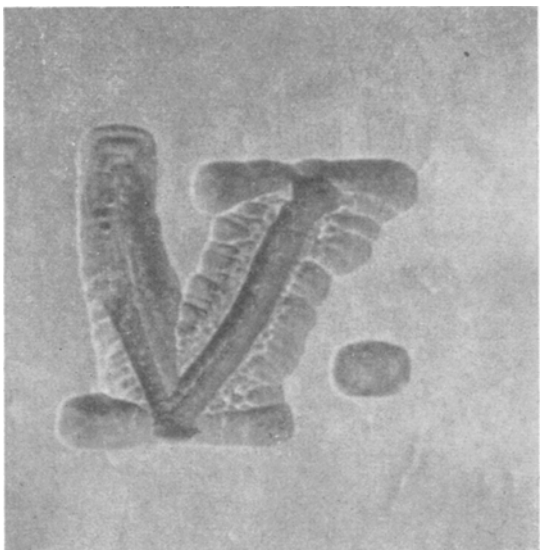

Figure 4 Band of etch pits around a scratch on (10.0). Etched in Li_2MoO_4/2% $LiBO_2$ for 10 min at ~800° C; *c*-axis is vertical in page (×178).

4.2. Emergent Pt Wires and Crystals

It is common for Pt crystals to nucleate on the surface of a BeO crystal at an intermediate growth stage and to grow with the subsequently enveloping BeO crystal. The Pt crystals may develop as large platelets or they may grow as fine, barely discernible threads; probably, there are also submicroscopic Pt threads in many of the crystals, With H_3PO_4 etchant, the remarkable etch pits shown in fig. 5 are formed at the points of Pt crystal emergence on {10.0}. The pit shapes are very asymmetrical along the *c*-axis, reflecting crystal polarity, and can be used to identify polarity orientation. Pt crystal emergences give rise to sharp pits on (00.1) and

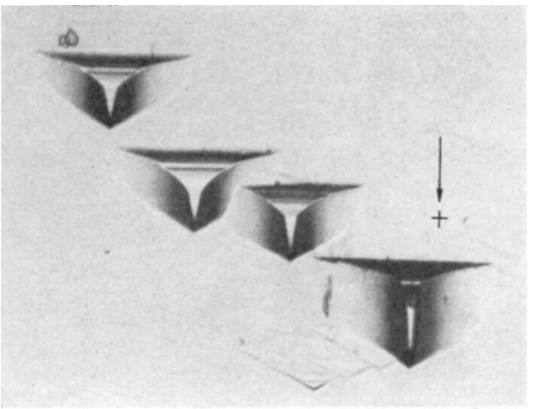

Figure 5 Asymmetrical pits at emergence of Pt threads on {10.0} formed by H_3PO_4; lower sharp tip of the pit coincides with the Pt thread (×16).

large hillocks on (00.$\bar{1}$, vic.) (fig. 6) with H_3PO_4 etchant. The hillocks are generally conical in shape, as shown in fig. 7, with an enclosed angle of ~90° at the apex. With a class-II etchant, the etching behaviour is reversed from that of H_3PO_4, in that emergent Pt threads on (00.$\bar{1}$, vic.) give rise to sharp, hexagonal etch-pits; on {10.0}, rectangular, sharp-bottomed pits are formed.

4.3. Inversion Twin

The crystals used here were primarily the prismatic and pyramidal crystals which were twinned by the presence of a slender axial core, whose crystallographic polarity was inverted relative to that of the enclosing crystal [10]. Although the experimental etching results are described in terms of this simple configuration, their extension to more-complex twin configurations is straightforward.

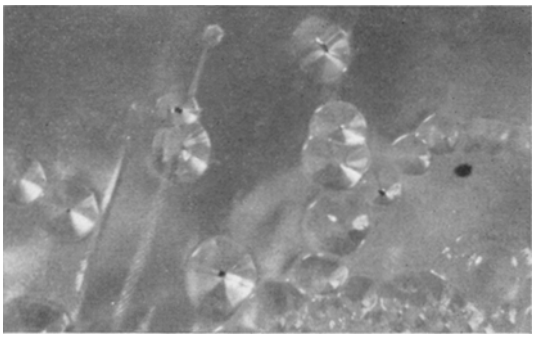

Figure 6 Hillocks formed, by etching in H_3PO_4 (~175° C), around Pt wires (black spots) on (00.$\bar{1}$, vic.) (×22).

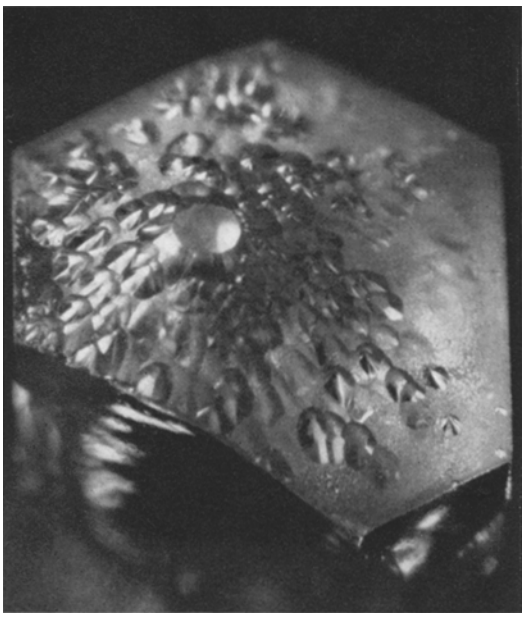

Figure 7 Growth face of prismatic crystal after moderate etching in H_3PO_4 (~175° C), showing etch-resistant termination face (00.1) on twin core, and etch-resistant hillocks on (00.$\bar{1}$, vic.) face (×16).

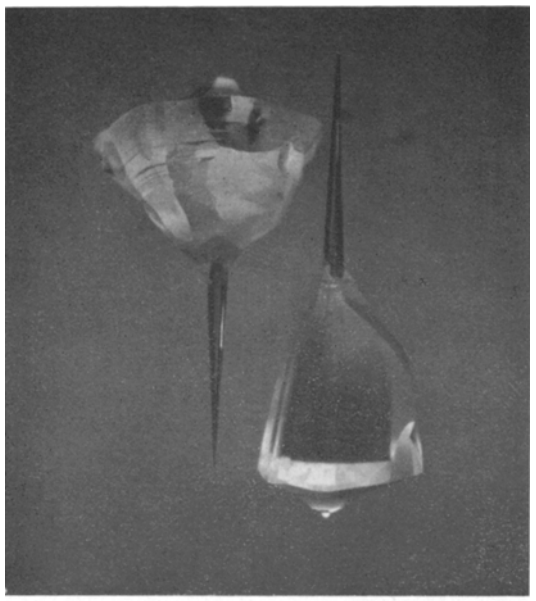

(a) (b)

Figure 8 Crystals after prolonged etching in H_3PO_4 (~175° C) showing prominent "tails" formed by etching pyramid faces away to expose twin core. Crystals were initially (a) pyramidal, and (b) prismatic with pyramidal termination (×10).

The etching morphology around the twin boundary due to prolonged etching in H_3PO_4 (~175° C) is especially remarkable. Fig. 8 shows a pair of crystals, one originally prismatic and the other originally pyramidal. In both cases, a "tail" was formed by rapid etching on {10.1}, thus exposing the etch-resistant core. Since the sides of the core are near-prismatic, which are relatively etch-resistant, the core is protected from dissolution. The core presents the rapidly etched negative (O) basal plane toward the tip of the exposed core, and, thus, it is surprising that the tip end is resistant to etching. Resistance to etching at the tip persists even after the tip has been ground away. In this case, a new centre of resistance to etching develops, around which a cone is formed by etching. Judging from correlation with X-ray diffraction topographic images [11], it appears that the centre of resistance is the point of surface emergence of the axial screw dislocation.

At the opposite end of the crystal, a compound slope is formed by H_3PO_4 (~175° C) between the (00.1) face terminating the twin core and the receding (00.$\bar{1}$, vic.) face. A cross-section sketch of the morphology in this case is illustrated in fig. 9. The slope of the narrow face

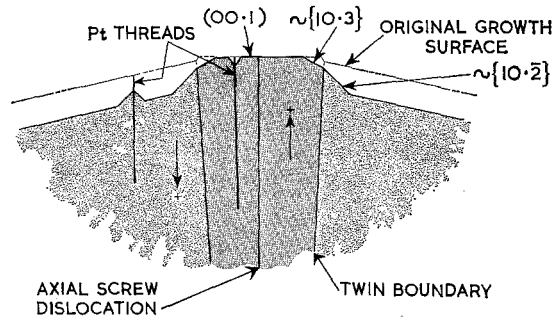

Figure 9 Sketch of etching morphology of growth face after prolonged etching in H_3PO_4 (~175° C), showing slopes formed adjacent to twin boundary and on hillock around Pt-thread emergent on (00.$\bar{1}$, vic.), and etch pit on (00.1) around emergent Pt thread.

between the boundary and the (00.1) face approximates to that for {10.3}. The slope of the broader face between the boundary and (00.$\bar{1}$, vic.) approximates to that for {10.$\bar{2}$}.

With class-II etchants, it is the exposed positive (Be) face that recedes rapidly, forming a deep, nearly flat-bottomed crater that extends across the entire diameter of the core. In addition to the dislocation-centred pit formed

on this face, the twin boundary also etches preferentially, thus forming a noticeable groove along the boundary at the edge of the crater floor. These features are illustrated as a sketch in fig. 3.

The trace of twin boundaries emergent on prism faces is also revealed by etching in either basic or acidic etchants. Fig. 10 is a photomicrograph of an etched boundary, appearing as a continuous groove on {10.0} after etching in H_3PO_4 ($\sim 175°$ C). Fig. 11 also shows a boundary groove on {10.0}, formed by class-II etchant. Etchability of the emergent boundary on this face is taken as direct evidence of a small, but significant, boundary energy [10].

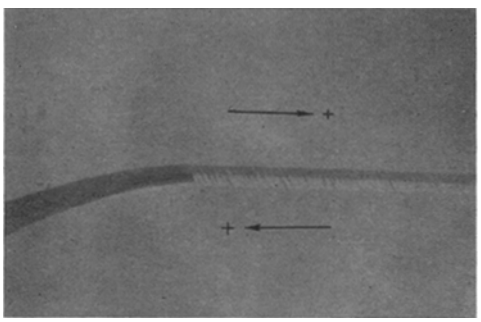

Figure 10 Groove along twin boundary on {10.0} after 10 min etch in H_3PO_4 ($\sim 175°$ C) ($\times 96$).

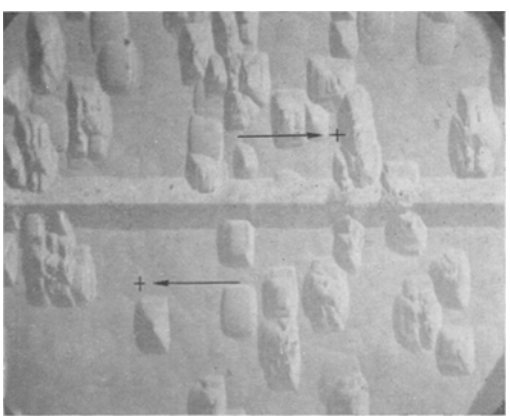

Figure 11 Etch pits and groove along twin boundary on {10.0} after 10 min etch in Li_2MoO_4/2% $LiBO_2$ at $\sim 800°$ C. Etch pits are attributed to surface bruise regions partly removed by this etch ($\times 186$).

4.4. Impurity Effects

The principal effect of point defects (impurities, vacancies, or other types presently unidentified), that are detectable by X-ray diffraction topography, is to give rise to etched surface texture in class-I etchants. Non-uniformity of point-defect concentrations as "growth strata" has been noted by topography [11]. These strata also are discernible as equatorial ridges on pyramidal faces after heavy etching in H_3PO_4 ($\sim 175°$ C), on both as-grown (fig. 8) and spherical crystals (fig. 2). The strata are detectable, under the same etching conditions, also on polished and etched (00.$\bar{1}$) faces. The intersections of the shallowly cone-shaped growth strata with the basal plane form a series of concentric rings. With etching, these rings become evident by the varying etch texture across the rings.

There did not appear to be any distinguishing gross impurity-related etch-figures or texture formed by either class-II or class-III etchants or by NaOH.

4.5. Surface Damage

Local surface-damage regions or bruises, due to intercrystal abrasion, give rise to etch figures that have been identified on some crystal faces. Etching of as-grown crystals in H_3PO_4 at 175° C forms isolated hillocks on the (00.$\bar{1}$, vic.) face. These hillocks, in part, are due to Pt inclusions (fig. 6); however, points of abrasion damage also appear to act as a retarding influence on dissolution resulting in essentially the same features, as seen in fig. 12. The initial topograph (fig. 12a) shows many, large, dark patches due to surface damage which persist at the tip of a hillock after immersion in the etchants (figs. 12b and 12c). In addition, not evident on the figure, a dense row of hillocks remains along the line of damage points on the edges formed by the (00.$\bar{1}$, vic.) and {10.0} faces. The isolated hillocks do not appear with etching on this face after it has been cut and polished, presumably because the more uniformly distributed surface damage leads to correspondingly more uniform etch-texture. The opposite basal face, (00.1), is normally resistant to etching in hot H_3PO_4, but the presence of local damage leads to etch-pitting, as evidenced by rows of etch pits formed on ground and lightly polished surfaces.

The class-II etchants also form flat-bottomed etch pits on (00.1) and {10.0} at points of surface damage (fig. 11). Assuming that the etch-pit depth is controlled by the initial depth of surface damage, the latter can be estimated from

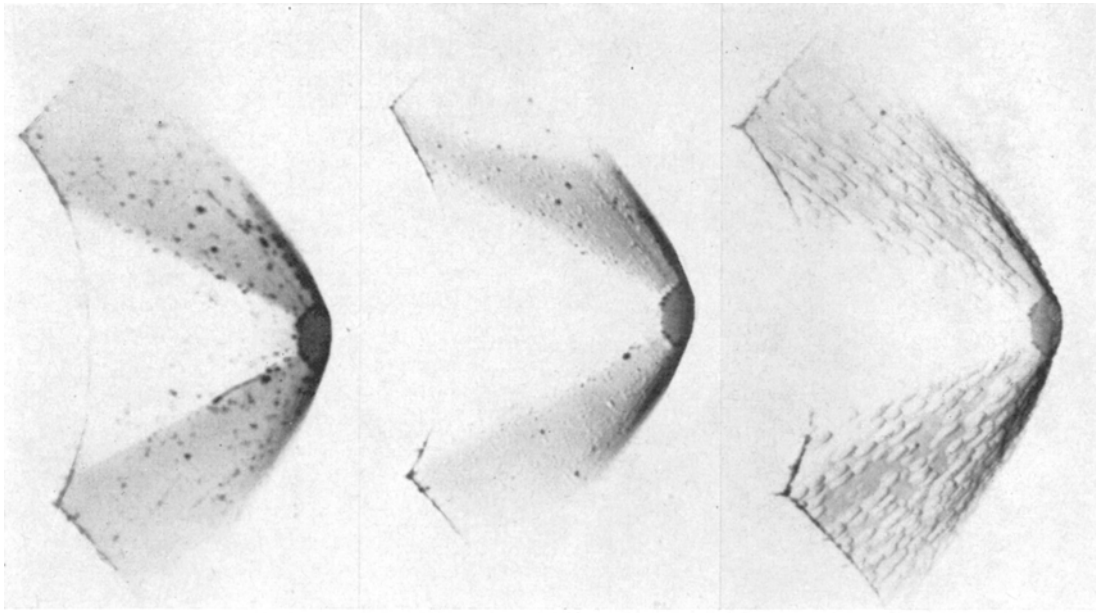

Figure 12 Berg-Barrett diffraction topograph ((00.2) reflection) of the growth end of a crystal: (a) before etching; (b) 1 min etch; (c) 3 min etch; in H_3PO_4 at ~175° C (×9).

measurement of pit depth. On both the above faces, damage depth was estimated to be about 15 μm. This is the same order of magnitude as the estimated 20 μm depth of damage due to grind-and-polish procedures.

5. Discussion

The crystallographically polar nature of BeO gives rise to some unusual aspects of morphology when BeO crystals are exposed to either acidic (class-I) or basic (class-II) etchants. The acidic etchants selectively attack O-rich (negative) basal faces, while the basic etchants preferentially attack the Be-rich (positive) basal faces. Etching selectivity also is strikingly evident in other ways: with the inversion twin exposed as a "tail" in one type of etchant, or as a relatively flat-bottomed crater in the other. These etching characteristics are generally consistent with models of etching phenomena previously presented [4, 14].

From a strictly practical standpoint, these data allow one to identify various types of surface-emergent crystal imperfections by visual inspection of etch figures produced by the described etchants. From the asymmetry of certain etch figures and of gross etching in either polar direction, the crystal polarity can be identified in the absence of any other indicator of polarity. Although these observations may be useful in guiding further etching studies with polycrystalline BeO, they cannot be applied directly without considerable reservation, because of the more complex defect arrays generally encountered in polycrystalline materials.

Although hydrofluosilicic acid is regarded as a class-I etchant, it was not given much attention in the present investigation, in view of the recent, careful study by Vandervoort and Barmore with reference to dislocations [7].

Etching effects usually are discussed in terms of dislocations; observations in the present studies show that other types of defects are important in giving rise to etch figures. One result was related to the heterogeneous distribution of Pt as enclosed thread-like crystals that could be revealed and located by etch figures. The Pt originated from the crucibles during growth of the host BeO crystals, and apparently was soluble enough in the flux to promote Pt crystal growth. It is reported occasionally that analysis of crystals grown in Pt-ware reveals the presence of Pt (for a recent example [15]). Development of suitable etchants may be valuable in revealing heterogeneity and locale of Pt in these other crystals.

Pt crystals such as these constitute line defects, as do dislocations, and in many cases cause the same type of etch figure. It is quite possible that, wherever Pt crystals form as thin, possibly submicroscopic, threads, the consequent etch figures could be mistakenly attributed to dislocations.

The other types of defects that generally have not been given attention are surface bruises and internal clouds of point defects, possibly impurities. These have been difficult to detect and localise prior to availability of X-ray diffraction topography, and hence their importance has not been recognised previously. The results of the present investigation reveal that these types of defects cannot be ignored in etching studies. The surface bruise or scratch type of defect can be considered as uncontrolled damage regions comparable to the more controlled indentations made in microhardness measurements, such as performed by Vandervoort and Barmore [7]. In either case, the etching effects can be attributed to the presence of dislocations in high local concentration close to the crystal surface.

It was determined also that at least one etchant composition ($Li_2MoO_4/NaPO_3$) can be used as a non-selective rapid etchant, and that at elevated temperatures (>1100° C) it also serves as a chemical polishing agent. This has been useful in removing surface damage due either to intercrystal abrasion or to cut-and-polish operations.

Appendices

1. Chemical Etchants for Single-Crystal BeO

1.1. Class I

1.1.1. Etchant		*Temperature*	*Time*
(*a*)	Phosphoric acid, H_3PO_4 (85%)	Room	100 h
(*b*)	H_3PO_4 (85%)	175° C	10 min
(*c*)	H_3PO_4 (85%)	175° C	1 h
(*d*)	Hydrofluosilicic acid, H_2SiF_6 + H_2O (1:6)	90° C	10 to 60 min
(*e*)	Hydrofluoric acid, HF	100° C	10 min

1.1.2. Action and Comments

(*a*) Only sign of etching attack is a fine, frosted surface on (00.$\bar{1}$,vic.).

(*b*) Shallow hillocks on {10.1}, elongated parallel to basal plane. Sharp, shallow hillocks on {11.1}, elongated parallel to *c*-axis projection. Somewhat deeper etch on polished $\{hk.\bar{l}\}$ faces than on $\{hk.l\}$ faces, if within ~15% of basal plane. Frosted etch on (00.$\bar{1}$, vic.) and on polished (00.$\bar{1}$). Angular etch features on (00.1) in polished section, presumed to be due to local structural damage (scratches, etc.). Sharpens relief at intersection of twin boundary with polished basal plane.

(*c*) Deep etching on (00.$\bar{1}$, vic.) with fine-textured, frosted surface; often leaving large hillocks with apex angle of ~90°, the hillock surface curved around central axis parallel to *c*-axis (fig. 7). Often these hillocks are associated with visible, emergent, Pt threads; others associated with surface damage (fig. 12). Sharp-bottomed, hexagonal pits formed on (00.1) at points of Pt-thread emergence, with curved sides ~{10.1}; damage spots etch out as flat-bottomed pits; otherwise (00.1) shows no sign of etching. Prism faces {10.0} are relatively etch-resistant except at Pt-thread emergence, where asymmetric pit is formed (fig. 5), and at damage regions. Very deep etching on {10.1}, yielding equatorial ridges reflecting internal growth strata of point defects, and progressively etching away to expose inversion twin core (fig. 8); when tip of exposed core is broken or ground-off, the exposed end usually etches to an equilibrium cone shape around an emergent screw dislocation as an etch-resistance centre. At emergence of twin boundary on growth face, two-valued slope forms, the break occurring at the boundary; slopes approximate {10.3} and {10.$\bar{2}$} (fig. 9). Twin-boundary emergent on prism face etches to form a groove (fig. 10).

(*d*) Basal plane etched after 10 min. First- and second-order prismatic and pyramidal faces etched after 20 to 60 min. (See Vandervoort and Barmore [7] for further details.)

(*e*) Etch in vapours. All surfaces frosted uniformly.

1.2. Class II

1.2.1. Etchant		*Temperature*	*Time*
(*a*)	Li_2MoO_4 + 2 to 10% MoO_3, V_2O_5, $LiBO_2$, or $Na_2B_4O_7$	800° C	10 min

continued from previous page

	Etchant	*Temperature*	*Time*
(*b*)	Li_2MoO_4 + 5 to 50% MoO_3, V_2O_5, $LiBO_4$, or $Na_2B_4O_7$	800° C	½ h
(*c*)	NaOH, saturated aqueous solution	50 to 100° C	24 h
(*d*)	NaOH	500° C	1 min
(*e*)	NaOH	800° C	10 min
(*f*)	KOH	600° C	1 h

1.2.2. Action and Comments

(*a*) Principal attack is on (00.1), forming sharp etch pit on emergent screw dislocation (fig. 3) and hexagonal, flat-bottomed pits on presumed damage regions. Shallow terrace etched rapidly from edges of plateau toward centre. Sharp pits formed on (00.$\bar{1}$, vic.) at emergent Pt crystals and dislocations initiated at inclusions. Sharp, rectangular pits formed on {10.0} at Pt crystal and edge dislocation emergence. Shallow, irregular etch-pits on all surfaces due to etching of surface bruises (fig. 11). Grooving along twin-boundary emergent on non-basal faces (fig. 11).

(*b*) General, unselective etch as with class-III etchant, except for rapid attack on (00.1), producing deep, broad crater on inversion twin core (fig. 3). Floor of crater shows pit on emergent screw dislocation as well as groove on twin boundary. Sharp, conical, deep pits on (00.1, vic.) due to emergent Pt crystals as well as on dislocations from inclusions (fig. 3). Etching more rapid with borate or vanadate than with MoO_3 additive.

(*c*) Etch rate strongly dependent upon temperature. Sharp etch pit on screw-dislocation emergent on (00.1). Shallow terrace rapidly etched from edge toward centre of (00.1) plateau. Distinctive, sharp, truncated-triangular pits on {10.1}.

(*d*) Etch pit formed on screw-dislocation emergent on (00.1). No other etch features noted.

(*e*) Uneven, deep attack on (00.1). On (00.$\bar{1}$, vic.), formation of many short "benches" bounded by (00.$\bar{1}$) and {10.$\bar{3}$} faces. On {10.1}, edge-shaped, pointed hillocks bounded by {10.1} faces. Rapid etch on all the above faces.

(*f*) Similar to NaOH at 800° C.

1.3. Class III

1.3.1. Etchant		*Temperature*	*Time*
(*a*)	$Li_2MoO_4/NaPO_3$	800° C	10 to 60 min
(*b*)	$Li_2MoO_4/NaPO_3$	1100° C	—

1.3.2. Action and Comments

(*a*) Nearly uniform etch on all surfaces, whether as-grown or polished, leaving slightly frosted surface texture and rounded corners. Removal rate ~(40 ± 10) μm/h (based on limited data, identity of crystal faces ignored). 20 μm adequate to remove surface damage due to grinding and polishing and to intercrystal abrasion.

(*b*) Uniform, smooth surface on all faces left by chemical dissolution.

2. Chemicals Unreactive Toward BeO

2.1. Experimental Conditions

Chemical	*Temperature* (° C)	*Time* (*h*)
Li_2MoO_4	800	½
Li_2MoO_4/10% LiF	800	½
$K_2S_2O_7$	600	1
K_2CO_3	600	1
4 N NaOH hydrothermal conditions	600	2
NaCl	800	1

Acknowledgements

The authors are grateful to J. W. Wagner, C. Griffith, T. D. Munsch, and F. J. Wittmayer for assistance in some of the etching experiments. These studies were sponsored by: the US Atomic Energy Commission; Fuels and Materials Branch, Division of Reactor Development and Technology, Contract AT(GEN-8)-11-1 (Atomics International); Contract No. W-7405-eng-48 (Lawrence Radiation Laboratory).

References

1. H. G. VAN BUEREN, "Imperfections in Crystals" (Interscience, New York, 1960), pp. 128-33.
2. J. W. FAUST, JR, "Etching of the III-V Intermetallic Compounds", "Compound Semiconductors", Vol. I (Reinhold, New York, 1962), pp. 445-68.
3. R. C. RAU, *J. Amer. Ceram. Soc.* **46** (1963) 484.
4. D. K. SMITH, H. W. NEWKIRK, and J. S. KAHN, *J. Electrochem. Soc.* **111** (1964) 78.
5. S. B. AUSTERMAN, D. A. BERLINCOURT, and H. H. A. KRUEGER, *J. Appl. Phys.* **34** (1963) 339.
6. S. B. AUSTERMAN, *Bull. Amer. Phys. Soc.* **7** (1962) 607.

7. R. R. VANDERVOORT and W. L. BARMORE, *J. Appl. Phys.* **37** (1966) 4483.
8. S. B. AUSTERMAN, *J. Nucl. Matls.* **14** (1964) 225.
9. H. W. NEWKIRK and D. K. SMITH, *Amer. Mineral.* **50** (1965) 44.
10. S. B. AUSTERMAN and W. G. GEHMAN, *J. Matls. Sci.* **1** (1966) 249.
11. S. B. AUSTERMAN, J. B. NEWKIRK, and D. K. SMITH, *J. Appl. Phys.* **36** (1965) 3815.
12. G. NOMARSKI and A. R. WERT, *Revue de Metallurgie* **52** (1955) 121.
13. G. G. BENTLE and K. T. MILLER, "Dislocations, Slip, and Fracture in BeO Single Crystals," *J. Appl. Phys.*, in press.
14. H. C. GATOS, *Science* **137** (August 1962) 3527.
15. A. A. BALLMAN, *J. Cryst. Growth* **1** (1967) 46.